Dynamics of Sounding Rockets at Burnout

WILLIAM C. WOMACK*
Transportation Technology, Inc., Denver, Colo.
AND
CHARLES W. BERT†
University of Oklahoma, Norman, Okla.
AND
FARRELL J. PERDREAUVILLE‡
Sandia Laboratories, Albuquerque, N. Mex.

This paper describes a new "integrated method" that allows sounding-rocket development engineers to determine the effects of various perturbing moments on the oscillatory motion of the vehicle. Furthermore, since a point-mass trajectory, aerodynamic pitching and damping coefficients, and an aeroelastic analysis are required for the basic vehicle design, the oscillatory analysis can be performed with very little extra effort. Analysis of a current rocket system by this method simulates the actual flight data very closely.

Nomenclature

A	= reference area
$\bar{A}_y, \bar{A}_z$	= mass-center acceleration components along y and z axes
C_{m_q}	= aerodynamic damping coefficient
F_y^*, F_z^*	= aerodynamic forces in y and z directions
$f_1(t), f_2(t)$	= coefficients for restoring and damping moments
$f_4(t), f_5(t)$	= coefficients for vibratory moments
g	= gravitational acceleration
I_{xx}, I_{yy}, I_{zz}	= mass moments of inertia about axes x, y, z
i	= index ($i = 2, 3$)
j, k	= indices referring to u_2, u_3 or r_2, r_3
J_{D_y}, J_{D_z}	= jet damping forces in the xy and xz planes
k	= index ($k = y, z$)
l	= reference length for C_{m_q}
$-l_1, l_2$	= positions of missile tail and nose, measured positive forward from the mass center
M	= total mass
M_{JD_k}, M_{q_k}	= jet and aerodynamic damping moments per unit pitch (or yaw) angle
$M_{r_2}^*, M_{r_3}^*$	= total moments about aeroballistic axes through mass center
P_{xy}, P_{xz}	= aerodynamic forces per unit length in xy and xz planes
q_j, q_k	= generalized coordinates; see Eqs. (1)
r_2, r_3	= pitch and yaw angles about aeroballistic axes
T^*	= motor thrust
t	= time
u_2, u_3	= displacements of missile relative to moving axes y and z
u_{2T}, u_{3T}	= u_2 and u_3 at tail
u'_{2T}, u'_{3T}	= slopes of missile at tail, in the xy and xz planes
x, y, z	= coordinates of moving-axis system
η	= inclination of x axis to vertical
ρ	= air density
τ_j, σ_k	= eigenfunctions for u_2, u_3 free-free-beam bending modes
ω_i	= circular frequency of the ith mode

Superscripts

dot $(\cdot)$	= derivative with respect to time

Received May 29, 1973; revision received April 19, 1974. This research is based on a dissertation submitted by W. C. Womack in partial fulfillment of the requirements for the Ph.D. degree at the University of Oklahoma, Norman, Okla.

Index categories: LV/M Dynamics, Uncontrolled; Sounding Rocket Systems.

* Project Manager.

† Professor and Director, School of Aerospace, Mechanical, and Nuclear Engineering. Associate Fellow AIAA.

‡ Member, Technical Staff.

PREVIOUS investigations of the dynamic characteristics of elastic rocket vehicles can be categorized into three types: 1) the pure theoretical approach,[1-3] 2) the similitude approach[4] which uses scale-model wind-tunnel tests, and 3) the flight-data correlation approach[5,6] where flight data are used to calculate effective values of aerodynamic parameters and the elasticity effects are estimated.

The purpose of this paper is to introduce a fourth approach that is called the integrated approach. The scheme is to use a set of differential equations that describe the motion of the elastic vehicle in such a manner that almost any part of the motion can be determined separately and combined along with other motions into the equations. These equations, derived in Ref. 7 and used in this paper, are similar in form to the equations derived by Young[8] for the planar case.

General Formulation

The following assumptions are made to simplify and define the problem: 1) mass and stiffness are functions of x only; 2) lateral bending is governed by linear, slender beam theory; 3) torsional rigidity is assumed to be infinite; 4) beam deflections relative to the moving axes are represented by normal-mode oscillations; 5) structural damping is neglected; 6) inclination of vehicle axis from the vertical is small; 7) elastic angles are small; 8) thrust misalignment is negligible; and 9) instantaneous mass moment of inertia can be approximated by the rigid-body one.

The missile configuration is described relative to a set of moving axes (x, y, and z) which has its origin fixed at the mass center. It is a right-handed orthogonal system that is fixed in the missile body and coincides with the undeflected missile principal axes, with the x axis directed along the longitudinal axis of symmetry of the undeflected missile.

The governing equations are presented, along with a brief explanation; a complete derivation is given in Appendix A of Ref. 7. The normal-mode displacement equations are

$$u_2(x,t) = \sum_{j=1}^{\infty} \tau_j \cdot q_j(t) \qquad u_3(x,t) = \sum_{k=1}^{\infty} \sigma_k \cdot q_k(t) \tag{1}$$

There is no equation for an element rotating about the x axis because of the assumption that the missile is rigid in the plane perpendicular to that axis. The equations of translational motion for the mass center are

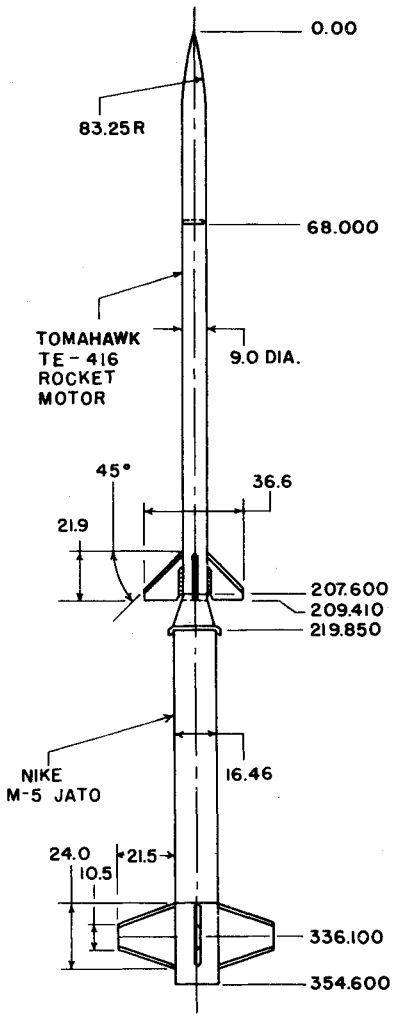

Fig. 1 The Nitehawk 9.[7] All dimensions are in inches.

$$\left.\begin{aligned} M\bar{A}_y &= T^*u'_{2T}+F_y{}^*-J_{Dy} \\ M\bar{A}_z &= T^*u'_{3T}+Mg\sin\eta-J_{Dz}+F_z{}^* \end{aligned}\right\} \quad (2)$$

It is more convenient to express the equations of rotational motion in terms of the "aeroballistic reference system." This is a system of axes that has its origin fixed at the mass center of the rocket and that pitches and yaws with the body but does not roll with it. The resulting equations of rotational motion are

$$I_{yy}\ddot{r}_2+I_{xx}\dot{r}_1\dot{r}_3 = M^*_{r_2} \qquad I_{zz}\ddot{r}_3-I_{xx}\dot{r}_2\dot{r}_1 = M^*_{r_3} \quad (3)$$

where

$$\left.\begin{aligned} M^*_{r_2} &= 57.3r_2f_1(t)-\dot{r}_2f_2(t)+r_2f_4(t) \\ M^*_{r_3} &= 57.3r_3f_1(t)-\dot{r}_3f_2(t)+r_3f_5(t) \end{aligned}\right\} \quad (4)$$

and

$$\left.\begin{aligned} f_1(t) &= T^*(u_{iT}-u'_{iT}l_1)-M_{r_2} \quad (i=2,3) \\ f_2(t) &= M_{JD_k}+M_{q_k} \quad (k=y,z) \end{aligned}\right\} \quad (5)$$

The equations for vibratory bending motion in the xz and xy planes are

$$\left.\begin{aligned} M(\ddot{q}_k+\omega_k{}^2q_k) &= \int_{-l_1}^{l_2} P_{xz}(x,t)\sigma_k(x)\,dx+T^*u'_{3T}\sigma_k(-l_1) \\ M(\ddot{q}_j+\omega_j{}^2q_j) &= \int_{-l_1}^{l_2} P_{xy}(x,t)\tau_j(x)\,dx+T^*u'_{2T}\tau_j(-l_1) \end{aligned}\right\} \quad (6)$$

Application to a Specific Vehicle

The purpose of the example is to demonstrate the use of the equations and to compare the motions obtained from the solution of the equations with actual flight data. This example is a typical second stage of the Nitehawk 9 in a typical trajectory during the period from motor burnout to exit from the atmosphere.[9]

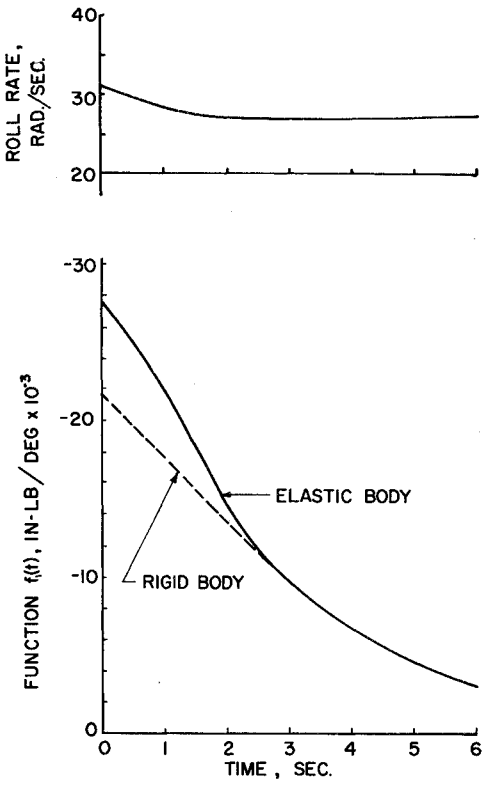

Fig. 2 Roll rate and function f_1 vs time.

Over-all dimensions of the Nitehawk 9 second stage are shown in Fig. 1. The vehicle is 207 in. long and weighs 255 lb at burnout. The payload is 68 in. long and weighs 125 lb. The vehicle has pitch and yaw moments of inertia of 335.0 slug-ft^2 each and a roll moment of inertia of 1.96 slug-ft^2. The vehicle mass center is located at station 105.6 in. The motion of the vehicle mass center is a point-mass trajectory for second-stage ignition at 12 sec.[9]

Using aerodynamic inputs from the typical trajectory, the aerodynamic loads are determined empirically using methodology and data from Ref. 10. The aerodynamic loading distribution is then used as input to the AEROMOD program, written by J. C. Weydert, Sandia Labs., Albuquerque, and documented in Appendix D of Ref. 7. This program calculates the body static deflection, the static margin of the vehicle, and the aerodynamic moment. Finally these results and the thrust are combined to obtain function $f_1(t)$ as shown in Fig. 2.

The aerodynamic damping moment is defined as[11]

$$M_{qk} = -\tfrac{1}{2}C_{m_q}\rho Al^2\dot{r}_iV_0 \quad (7)$$

From the work of Curry and Uselton,[12] $C_{m_q} = 600$ rad^{-1} for the Nitehawk 9 upper stage at Mach 8. The values of M_{qk} were calculated as shown in Table 1.

Table 1 Aerodynamic damping moment vs time

Time, sec	M_{qk}, lb-ft
0	892
0.5	780
1.0	665
2.0	456
3.0	298
4.0	210
5.0	140
6.0	96

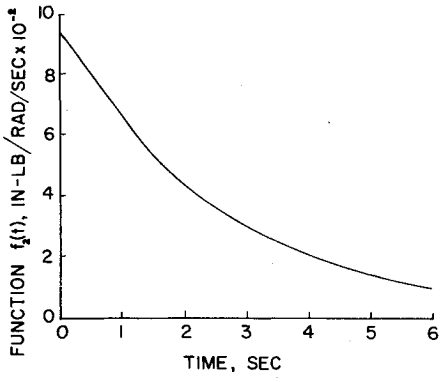

Fig. 3 Function f_2 vs time.

The jet damping moment is defined as[13]

$$M_{JD_k} = -2\omega_k \dot{M} l \tag{8}$$

The calculated jet damping moment per unit angular rate decreased only slightly in the first 0.5 sec and then rapidly attenuated to zero within a total time of only 0.94 sec.

From the work of Reis and Sundberg,[5] it is assumed that the lateral displacement of the payload mass center is 0.143 in. from the launch-vehicle centerline. This induces a force of 35.5 lb and by virtue of a 5.5 ft moment arm from the vehicle mass center, a moment of 195 lb-ft.

Stone[14] demonstrated the possibility of a nonlinear magnus moment as the cause of exoatmospheric coning motion, while Curry and Uselton[12] hypothesized a moment caused by asymmetric lee-side vorticity. However, since there are no reliable methods available for predicting these moments, here they are arbitrarily assumed to be small, 200 lb-ft.

The vibratory angular displacement is calculated by means of the Sandia SHOCK Code,[15] assuming that the vibratory motion is caused by the tailoff of the thrust vs time curve as burnout is approached.

In representing the mechanical characteristics of the vehicle, two mathematical models are considered. In the first model, the vehicle is treated as a continuous beam with mass and flexural rigidity varying along its length, using data presented by Witte.[16] The resulting motion is nearly sinusoidal with a constant bias and a frequency of 30 Hz, which is very near the fundamental bending frequency of the vehicle, 32 Hz, as determined experimentally by Witte.[16]

In the second model, the joint at the payload attachment is assumed to be loose. Various possible causes for such a loose joint include manufacturing tolerances, lack of tightening in the field, and differential thermal expansion due to aerodynamic heating. Reis and Sundberg[5] showed that the latter cause could reduce the joint rotational spring rate to approximately 10^6 lb-in./rad. Using this value, the code predicted a primary motion with a frequency of approximately 4.3 Hz with a superimposed higher-frequency fluctuation of small amplitude which is neglected hereafter. Witte[16] found that the experimentally measured fundamental frequency in the presence of a loose joint varied from 2–32 Hz. The deflection of the body and the vibratory motions result in moments that are applied to the moment equations. These two moments and all other moments were determined in Ref. 7.

The functions $f_4(t)$ and $f_5(t)$ appearing in Eqs. (4) are taken to be

$$f_4(t) = 0.0015 + 0.005 \sin \omega t, \quad \omega = 188 \text{ rad/sec or } 27 \text{ Hz}$$

$$f_5(t) = 0.0015 + 0.005 \cos \omega t$$

The roll rate vs time, $f_1(t)$, and $f_2(t)$ are shown in Figs. 2 and 3. The following initial conditions, based upon Tomahawk coning flight 152-45, are assumed

$$r_2(0) = \dot{r}_3(0) = 0; \quad r_3(0) = 0.035 \text{ rad}$$

$$\dot{r}_2(0) = 0.882 \text{ rad/sec}$$

Results and Discussion

Yaw-gyro traces from Nitehawk 9 flights showing normal, locked in (or roll-pitch coupled), and coning motion are shown in Fig. 4 (from Ref. 12). In attempting to duplicate these motions, the approach was to use the same relatively standard restoring moments (function f_1) and aerodynamic damping moments (function f_2) as used for the normal flight. The other conditions are then added to duplicate the locked in and coning flights.

Figure 5a shows the computer simulation of the normal[17] or desired flight. It can be seen that the computer flight data simulate the actual flight data quite well. The vehicle has slight oscillatory motion at burnout; it damps slightly and then diverges slightly as the vehicle leaves the atmosphere. Figure 5b shows a

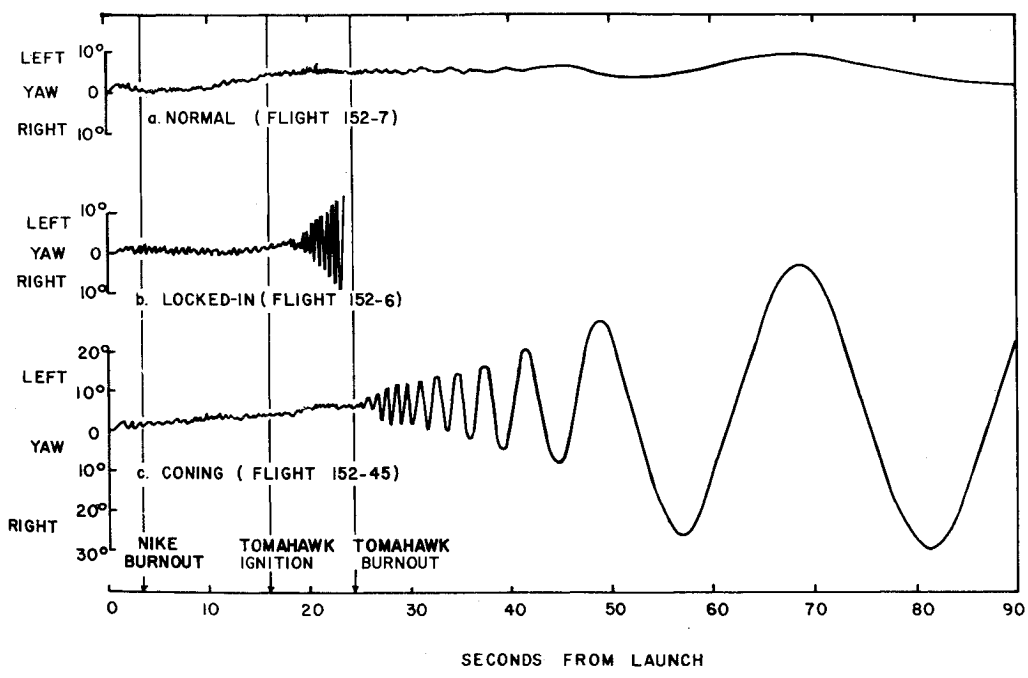

Fig. 4 Yaw-gyro traces from Nitehawk flights showing normal, locked-in, and coning motion.

simulation of roll-pitch coupling. The motion is highly divergent when the roll rate coincides with the pitch frequency. The bent payload moment was used as the disturbing moment to cause the two frequencies to lock together.

The difficult motion to simulate is the coning motion. Several different attempts were made to duplicate the motion on the computer. The different cases are as follows

Case 1

Figure 5c shows the simulated motion with the bent payload moment as the only additional applied moment. It is seen that the bent payload has very little effect on the motion.

Case 2

Figure 5d shows the simulated motion with the arbitrary moment applied. Although the oscillation tends to drift off from the line of flight, there is little increase in coning motion.

Case 3

Figure 6a shows the motion caused by applying both the bent payload moment and the arbitrary moment. There is little or no effect on the motion.

Case 4

Using the vibratory moment caused by the continuous vehicle (no loose joint), no noticeable difference between the resulting motion and the normal flight motion is found. When the bent payload moment is applied in addition to the vibrational moment, the resulting motion is identical to that in Case 2.

Case 5

Figure 6b shows the motion of the vehicle using the vibratory moment caused by the vehicle with a loose payload. Since the payload can bend, the moment caused by the mass offset is also included. The vibratory motion couples with the rolling motions and the yaw angle (and hence the pitch angle) begins to get larger. Using conservation of angular momentum, it is predicted that the yaw angle will grow to a value of 10–15° as the vehicle leaves the atmosphere and no longer has restoring and damping moments.

Case 6

Figure 6c shows the motion of the vehicle with the bent payload, its vibratory motion and the arbitrary moment all combined, i.e., simply a superposition of the motions of Cases 2 and 5. The motion tends to drift off from the line of flight and the yaw angle grows to the predicted 10–15°.

The Nitehawk 9 flight performance specification[9] limits the maximum allowable coning angle to $\pm 5°$. About 25% of the test units failed to meet this requirement by varying amounts. Most of the units that had large coning angles attained angles between ± 10 and $\pm 30°$; Flight 152-45 had a coning angle of $\pm 30°$, which was typical of these. This case does cause coning and duplicates the flights having smaller coning angles, but does not account for the larger coning angles.

Case 7

All input moments were increased to larger values in an attempt to duplicate the flight data for larger coning angles. The only duplication obtained occurred when the vibratory input with the loose payload was increased by a factor of four, i.e., the input was changed to $(0.0015 + 0.02 \sin \omega t)$. See Fig. 6d.

The motion obtained was virtually identical to the large-coning-angle flight data. It is an interesting observation but one that is difficult to duplicate in actual flight conditions. The accelerometers flown in most small rockets do not measure data at frequencies below 50 Hz. Thus, although the computer simulation duplicates the flight data, there is no assurance that such a vibratory environment exists in actual flight. Of course, the magnitude of the vibration may be somewhat greater than those calculated simply because only the thrust-induced vibrations were considered. This flexible joint reasoning is strengthened further by the fact that the coning was greatly reduced by stiffening the payload separation joint.

Case 8

To determine the effects of reducing the aerodynamic coefficients, functions f_1 and f_2 were reduced in steps. A 20% reduction in f_1 (restoring moment) did not increase the magnitude of the oscillation angle but did reduce the frequency slightly. However, a 20% reduction in f_2 (damping moment) caused the system to diverge without any disturbing moment.

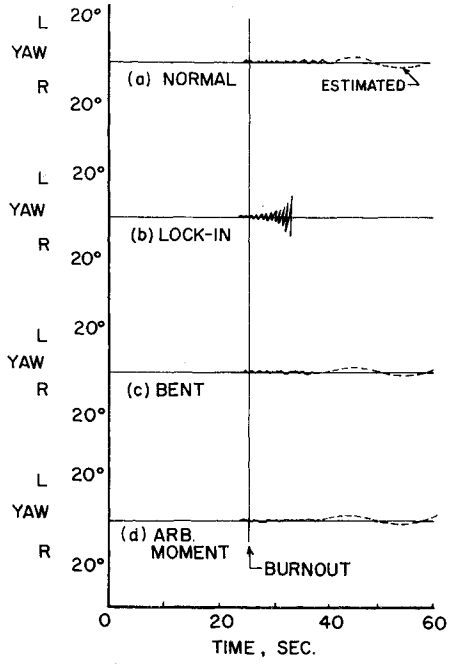

Fig. 5 Simulated yaw data.

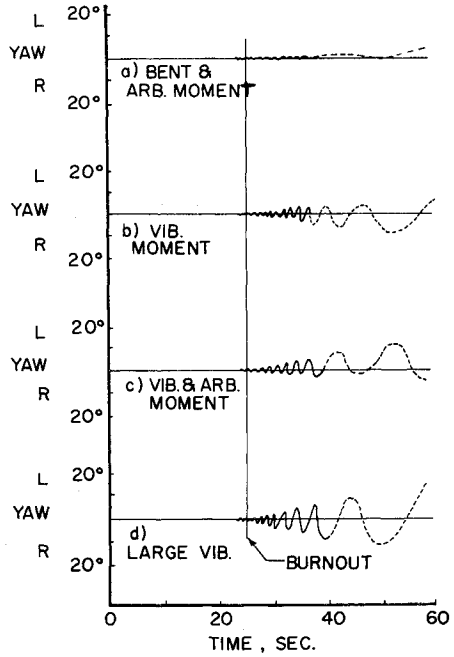

Fig. 6 Simulated yaw data (continued).

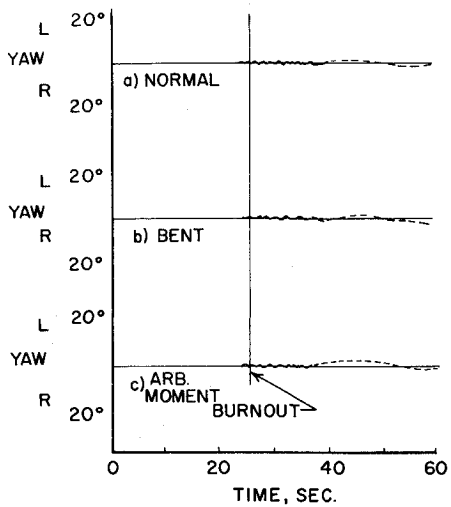

Fig. 7 Simulated yaw data corresponding to rigid-body motion.

In an attempt to get a complete comparison, the rigid-body motions were run on the analog. The rigid-body motion was determined using $f_1(t)$ from Figs. 2 and 3. Figure 7a shows the resulting motion of the rigid vehicle with the standard restoring moments and aerodynamic damping moments. With the same initial conditions as used in the flight shown in Fig. 5a, the rigid-body motion is almost identical to the normal elastic flight. The final amplitude of the rigid-body motion is slightly smaller than the elastic motion and the frequency is different. At 2.0 sec after burnout, the rigid-body frequency was 2.5 Hz while the elastic-body frequency was 2.75 Hz.

The rigid-body motion was also determined using an applied moment caused by a bent rocket and the arbitrary moment; see Figs. 7b and c. It should be noted that these motions are very similar to their corresponding cases in the elastic-body motion, Figs. 5c and d. Apparently the only large effect on the total motion of the vehicle was caused by coupling of the vibratory and yawing motions.

Conclusions

The integrated approach provides a new and powerful tool to determine the effects of various perturbing moments on the oscillatory motion of the vehicle. Furthermore, since a point-mass trajectory, aerodynamic pitching and damping coefficients, and an aeroelastic analysis are required for the basic design of a vehicle, the oscillatory analysis can be performed with little extra effort.

The results of the analysis of the Nitehawk 9 by this method agree well with limited actual flight data. They indicate that the extra-atmospheric coning of the Nitehawk may be caused by the coupling of the vibratory and roll motions. It is shown that variations in the restoring moments have very little effect on the magnitude of oscillations but that the frequency of oscillation is affected; however, lowering the damping moment causes the oscillations to grow.

References

[1] Meirovitch, L. and Wesley, D. A., "On the Dynamic Characteristics of a Variable-Mass Slender Elastic Body Under High Accelerations," CR-713, Feb. 1967, NASA.

[2] Meirovitch, L., "General Motion of a Variable Mass Flexible Rocket with Internal Flow," *Journal of Spacecraft and Rockets*, Vol. 7, No. 2, Feb. 1970, pp. 186–195.

[3] Meirovitch, L. and Bankovskis, J., "Dynamic Characteristics of a Two-Stage Variable-Mass Flexible Missile with Internal Flow," CR-2076, June 1972, NASA.

[4] Hanson, P. W. and Doggett, R. V., Jr., "Aerodynamic Damping of a 0.02-Scale Saturn SA-1 Model Vibrating in the First Free-Free Bending Mode," TN D-1966, Sept. 1963, NASA.

[5] Reis, G. E. and Sundberg, W. D., "Calculations of the Aeroelastic Bending of a Sounding Rocket Based on Flight Data," SC-R-67-1025, March 1967, Sandia Labs., Albuquerque, N.Mex.

[6] Baines, D. J. and Pearson, K. G., "Aeroelasticity as a Consideration in Aerodynamic Design of Rolling, Unaugmented Research Rockets," *Journal of Spacecraft and Rockets*, Vol. 4, No. 12, Dec. 1967, pp. 1603–1608.

[7] Womack, W. C., "The Dynamics of Sounding Rockets at Burn Out," Ph.D. dissertation, 1971, Univ. of Oklahoma, Norman, Okla.

[8] Young, D., "Generalized Missile Dynamics Analysis II—Equations of Motion," GM-TR-0165-359, April 1958, Space Technology Labs., Los Angeles, Calif.

[9] Womack, W. C., "Nitehawk 9," SC-DR-65-456A, Jan. 1966, Sandia Labs., Albuquerque, N.Mex.

[10] Muraca, R. J., "An Empirical Method for Determining Static Distributed Aerodynamic Loads on Axisymmetric Multistage Launch Vehicles," TN D-3283, March 1966, NASA.

[11] Davis, L., Jr., Follin, J. W., Jr., and Blitzer, L., *Exterior Ballistics of Rockets*, Van Nostrand, Princeton, N.J., 1958.

[12] Curry, W. H. and Uselton, J. C., "Some Comments on the Aerodynamic Characteristics of the Tomahawk Sounding Rocket," SC-R-66-997, March 1967, Sandia Corp., Albuquerque, N. Mex.

[13] "Six-Degree-of-Freedom Flight-Path Study Generalized Computer Program, Pt. I—Problem Formulation," FDL-TDR-64-1, 1964, Air Force Flight Dynamics Lab., Wright-Patterson Air Force Base, Ohio.

[14] Stone, G. W., "The Angular Motion of a Rocket-Propelled Vehicle in Free Flight," SC-RR-66-42, Aug. 1966, Sandia Labs., Albuquerque, N. Mex.

[15] Gabrielson, V. K. and Reese, R. T., "SHOCK Code User's Manual—A Computer Code to Solve the Dynamic Response of Lumped-Mass System," SCL-DR-69-98, 1969, Sandia Labs., Livermore, Calif.

[16] Witte, A. F., "Investigation of Bending Modes in a Single Stage Tomahawk System," T-12026, 1966. Sandia Labs., Albuquerque, N.Mex.

[17] Stone, G. W., "Aerodynamic Analysis of the Sandia Nitehawk 9 Rocket System," SC-RR-66-665, Feb. 1966, Sandia Labs., Albuquerque, N. Mex.